frontiers | Frontiers in Marine Science

TYPE Original Research
PUBLISHED 06 August 2025
DOI 10.3389/fmars.2025.1644888

OPEN ACCESS

EDITED BY
Haosheng Huang,
Louisiana State University, United States

REVIEWED BY
Guoxiang Wu,
Ocean University of China, China
Junliang Gao,
Jiangsu University of Science and Technology, China

*CORRESPONDENCE
Jianjun Zhou
zhoujj@tsinghua.edu.cn

RECEIVED 11 June 2025
ACCEPTED 22 July 2025
PUBLISHED 06 August 2025

CITATION
Sun J, Zhang M and Zhou J (2025) Tidal responses of the semi-enclosed Bohai Sea to the long-term expansion of the Yellow River Delta.
Front. Mar. Sci. 12:1644888.
doi: 10.3389/fmars.2025.1644888

Tidal responses of the semi-enclosed Bohai Sea to the long-term expansion of the Yellow River Delta

Jiayue Sun, Man Zhang and Jianjun Zhou*

Department of Hydraulic Engineering, Tsinghua University, Beijing, China

River deltas, formed by fluvial sediment accumulation, act as dynamic interfaces between land and sea. The Yellow River Delta (YRD) has prograded rapidly into the semi-enclosed shallow Bohai Sea (BS) over the past century. While tidal dynamics are recognized as key drivers of estuarine morphology and ecology, it is unclear how and to what extent this deltaic expansion impacts the tidal regime in the BS. This study investigates the tidal responses of the BS to both historical (circa 1855, 1962, 1981, 2003) and projected century-scale delta coastline advancement, utilizing numerical simulations and theoretical analysis. The results indicate that the seaward expansion of the delta alters tidal resonance patterns, inducing tidal responses in a nonlinear way across the BS. Specifically, historical delta expansion enhanced tidal flux and currents monotonically across major bays in the BS, whereas future sedimentation over the coming decades leads to an overall reduction in tidal dynamics. Locally, tidal currents and sediment transport capacity are expected to increase around the active lobe owing to river mouth protrusion at the expense of having the river base level raised; they decrease near the abandoned lobes with standby river courses, potentially hindering sediment dispersal and threatening the delta's morphological stability. Furthermore, the basin-scale tidal weakening caused by the delta expansion may diminish water exchange capacity in the BS, posing challenges for ecological environment and economic services.

KEYWORDS

tidal dynamics, Bohai Sea, delta progradation, Yellow River Delta, tidal resonance

1 Introduction

River deltas serve as crucial interfaces between terrestrial and marine environments, shaping unique landscapes and support productive ecosystems (Tessler et al., 2015; Nienhuis et al., 2020). Fluvial-dominated deltas with weak tidal dynamics, such as the Mississippi and Yellow River deltas formed by sediment-laden rivers discharging into semi-enclosed bays, often experience rapid progradation due to sediment accumulation near river mouths (Passeri et al., 2015; Xu et al., 2019; Zhang et al., 2022b). The seaward

expansion of deltas not only reshapes coastal landscapes but also modifies the geometry and hydrodynamics of adjacent bays (Talke and Jay, 2020; Zhang et al., 2023). These changes highlight the delta and adjacent marine region as a sensitive and dynamically coupled system.

The Yellow River (YR) is renowned for its high sediment load, with an average of 1.2×10^9 t/a of sediment delivered to the Bohai Sea (BS) in pre-damming period. Approximately 74%-98% of the sediment is deposited within the delta plain and subaqueous delta due to weak tidal dynamics (Qiao et al., 2016; Zhou et al., 2020; Bi et al., 2021). As a result of rapid sedimentation in the floodplain, the modern Yellow River Delta (YRD) has gained over 5400 km^2 of land since the river shifted from the Yellow Sea to the BS in 1855, with an average accretion rate of 22 km^2 per year (Zheng et al., 2017; Ji et al., 2022). Over the last half century, reduced sediment delivery due to anthropogenic activities have decelerated the overall delta progradation (Jiang et al., 2017; Ji et al., 2020; Fu et al., 2021). However, the active deltaic lobe has continued to extend seaward since the river flow has been stabilized through the Qingshuigou channel in 1976, with the mean rate of 0.83 km/a (Kong et al., 2015; Bi et al., 2021). During the dramatic morphological evolution of the YRD, earlier works have examined the spatial and temporal changes in tidal dynamics around the delta during specific historical periods under assumed constant tidal conditions in the BS (Wang et al., 2015; Bai et al., 2019; Zhan et al., 2020; Miao et al., 2022; Zhang et al., 2023). Most of them focused on short-term changes (spanning several decades) and were limited to the nearshore areas of the delta, while overlooking potential alterations in the overall tidal regime of the BS. As climate is cyclical and the retention capacity of sediment trapping projects upstream is limited (Kong et al., 2016; Wang et al., 2016; Guo et al., 2021), a future increase in sediment supply from the YR is very likely, which may further accelerate the delta expansion. A comprehensive investigation of tidal evolution in the BS throughout the historical and projected expansion of the YRD remains lacking, which is critical for the stability of both inland and coastal regions.

The Bohai Sea is a semi-enclosed continental sea characterized by shallow water, strong damping effects, and convergent geometry (Pan et al., 2022). Tidal dynamics in such semi-enclosed bays are highly sensitive to changes in coastline and geomorphology (Talke and Jay, 2020; Juarez et al., 2025). Previous studies have indicated that coastline changes by anthropogenic activities, including reclamation, construction of seawalls and navigation projects, significantly affected the propagation, reflection and dissipation of tidal waves, and could alter the resonant properties of the semi-enclosed bay (Pelling et al., 2013; Zhu et al., 2018; Lu et al., 2022; Wu et al., 2023b). In particular, the resonance is a common hydrodynamic phenomenon in bays or harbors, occurring when the incident wave period aligns with the basin's oscillation period, which depends on the water depth, bottom friction, and geometric configurations (Ensing et al., 2015; Gao et al., 2021, Gao et al., 2024). Morphological modifications can thus shift the resonance state, amplifying or damping tidal responses. Such effects may exacerbate water level oscillations and damage coastal infrastructures (Gao et al., 2020; Juarez et al., 2025), or conversely reduce tidal flux, weakening water exchange capacity and contributing to ecological degradation (Zhu et al., 2018; Liu et al., 2023a; Wu et al., 2023b). While existing studies have focused primarily on anthropogenic shoreline changes, the expansion of the YRD, protruding into the BS, has also profoundly reshaped the regional coastline. However, the extent and mechanisms of its impact on tidal dynamics in the BS remain unclear. Given the intrinsic vulnerability of the semi-enclosed bay to morphodynamic adjustments, the long-term delta expansion may induce strong and far-reaching tidal responses in the BS, with important implications for coastal resilience and sustainable management.

The primary objective of this study is to investigate and quantify the tidal responses in the BS to the long-term expansion of the YRD. Specifically, the coastline evolution of the YRD since 1855 was analyzed using data culled from the literature. Then the tidal dynamics under different delta coastlines caused by historical (circa 1855, 1962, 1981, 2003) and future (over the next 107 years) progradation were examined using a large-scale hydrodynamic model. Furthermore, the mechanisms driving the tidal responses and the potential implications for the coastal region were discussed. The insights gained from this study can be conducive to provide scientific implications for the sustainable development of other large deltaic and coastal systems.

2 Materials and methods

2.1 Study area

The Yellow River Delta is characterized by high sediment load, fast accretion and frequent avulsions (Figure 1A). Over the last 2000 years, the sediment delivered by the YR was $1–1.1 \times 10^9$ t/a (Milliman and Syvitski, 1992; Ganti et al., 2014). The lower course of the YRD has shifted more than 1593 times from 602BCE to 1938CE (according to the Yellow River Conservancy Commission). Since 1855, the modern YRD has prograded seaward at an average rate of approximately 150 m/a (Vangelder et al., 1994), accompanied by over 50 shifts of deltaic river courses (Zheng et al., 2017). Currently, three large artificial diversions of the main channel in the YRD were implemented since 1953. The deltaic channel has migrated from Shenxiangou (SXG) course (1953-1964) and Diaokouhe (DKH) course (1964-1976) to Qingshuiogu (QSG) course (1976-present). The active delta lobe has expanded seaward consistently since 1976, forming a spit-like feature extending 20 km seaward (Pelling et al., 2013).

The Bohai Sea is a semi-enclosed continental shelf sea situated in the northeastern region of China. Adjacent to megacities and hosting significant oil fields, it acts as a focal point for extensive economic and maritime activities (Tian et al., 2020; Wang et al., 2021). There are five regions in the BS: Liaodong Bay (LDB), Bohai Bay (BHB), Laizhou Bay (LZB), the central area, and Bohai Strait,

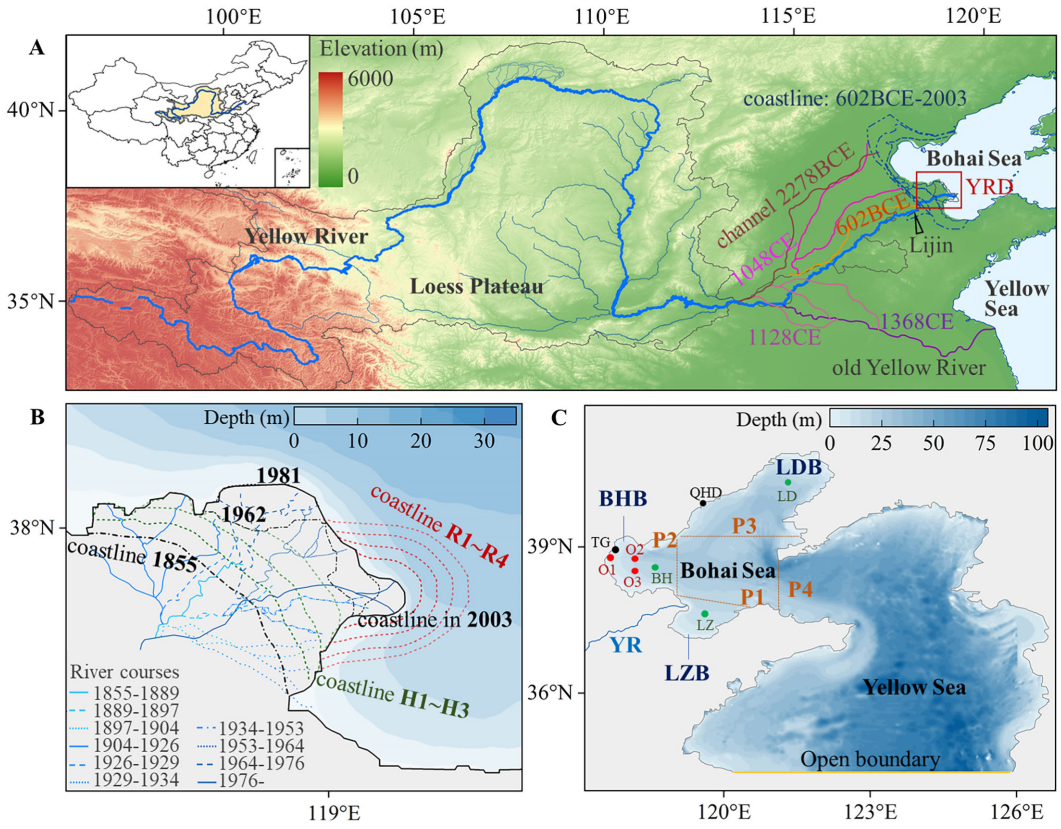

FIGURE 1
Location of the study area. **(A)** Map of the Yellow River Basin, showing the historical lower reaches and coastline evolution over the past thousand years. **(B)** The modern Yellow River Delta. Blue lines: the river courses since 1855 conducted by YRCC. Black lines: historical delta coastlines. Red lines: projected delta coastlines. Green lines: hypothetical historical coastlines used to fill data gaps between 1855 and 1962. **(C)** Bathymetric map of the Bohai Sea, showing the model domain. P1-P4: cross-sections in Laizhou Bay, Bohai Bay, Liaodong Bay, and Bohai Strait. Red circles: stations recording water level and velocity (O1-O3). Black circles: stations recording tide level (TG, QHD). Green circles: typical points for uncertainty analysis (LZ, BH, LD).

which connects the BS to the northern Yellow Sea (Figure 1C). It spans approximately 555 km from northeast to southwest and about 350 km from west to east, covering a total area of 77000 km² with an average depth of 18 m (Wang et al., 2022). The tidal regime in the BS is dominated by irregular semi-diurnal tides, with the M_2 constituent being the principal tidal component (Lu et al., 2022). The tidal dynamics are relatively weak, characterized by an average tidal amplitude of 2 m and an average tidal flow velocity of 0.5–1.0 m/s (Wu et al., 2023a).

2.2 Data source

The dataset of daily flow and sediment load at the Lijin station (the most downstream hydrological station on the YR) was measured and provided by the Yellow River Conservancy Commission (YRCC). The shoreline and bathymetry data since 1962 were obtained and digitized from marine charts published by the Navigation Guarantee Department of the Chinese Navy Headquarters. The shoreline and bathymetry data in 1855 were digitized from the bathymetric maps studied by Wang and Huang (1988). These data were georeferenced and corrected to the same datum (corresponding to the low tide line). The static shoreline representation omits the differences between high and low tide lines. The mean width of intertidal zones along the YRD is approximately 2 km (Fan et al., 2018; Wang et al., 2020; Cao et al., 2023), spanning about one cross-shore grid cell at the model resolution. Considering the basin-scale focus of this study, the impact of using static shorelines on the overall tidal response is limited. This approach provides a consistent and measurable boundary for long-term modeling. Additionally, data of the delta land area was culled from the literature, which was extracted from remote-sensing satellite images and bathymetric surveys (Tang et al., 2020; Fu et al., 2021).

The water level and velocity (speed and direction) data used for model validation were collected through a field survey conducted during July 13-16, 2003. These datasets were obtained at three stations, O1 (117.73°E, 38.88°N), O2 (118.12°E, 38.85°N), and O3 (118.12°E, 38.58°N) (Figure 1C). Measurements were taken using a Conductivity-Temperature-Depth (CTD) and an Acoustic Doppler Current Profilers (ADCP), respectively. Tide levels at TG (117.78°E, 38.98°N) and QHD (119.62°E, 39.92°N) were obtained from tide tables during November 15-17, 2012.

2.3 Hydrodynamic model

2.3.1 Model setting and validation

The tidal dynamics were investigated by developing a large-scale hydrodynamic model using Delft3D, which has been widely applied in rivers, estuaries, and coasts (Morovati et al., 2023; Ayyappan et al., 2024). The simulation domain covers the entire BS and the northern region of the adjacent Yellow Sea (Figure 1C), which covers the area from 117.5° E to 126.9° E in longitude and from 34.4°N to 41.0° N in latitude. The domain facilitates analysis of tidal responses throughout the BS. The area is discretized into the rectangular grid with resolutions of 1.5 km in the longitudinal and latitudinal directions. The open boundary is set on the 34.4°N latitude in the northern Yellow Sea, sufficiently far from the YRD to eliminate possible boundary effects. The tidal harmonic constants of nine tidal components (M_2, S_2, N_2, K_2, K_1, O_1, P_1, Q_1, and M_4) obtained from a global scale ocean model, the TPXO7.2 model (Egbert and Erofeeva, 2002), are used to calculate the time series of water levels along the open boundary. The model adopts the cold start method with a time step of 5 minutes, and is run for a simulation period of 1 year.

The calculated results are validated by comparing them with field observations. The accuracy of the simulations is quantified using two metrics, Root-Mean-Square Error (RMSE) and Nash-Efficiency (NSE) (see Equation 1, 2):

$$RMSE = \sqrt{\frac{\sum_{i=1}^{N}(X_{OBSi} - X_{MODi})^2}{N}} \quad (1)$$

$$NSE = 1 - \frac{\sum_{i=1}^{N}(X_{OBSi} - X_{MOD_i})^2}{\sum_{i=1}^{N}(X_{OBSi} - \overline{X}_{OBS_i})^2} \quad (2)$$

where X_{OBSi} is the measured value, X_{MODi} is the simulated value, $\overline{X}_{OBSi}$ is the average of the measured value, N is the total number of samples. Simulated water levels in stations O1-O3 are shown in Figures 2A–C, with the RMSE values of 0.20-0.23 m and the NSE values of 0.92-0.96. The RMSE values of tide speed and direction are below 0.13 m/s and 39.6°, respectively, with the corresponding NSE values exceeding 0.85 and 0.82 (Figures 2D–I). Simulated tide levels at TG and QHD also exhibit strong agreement with the measurements, with the RMSE values below 0.15 m and the NSE values above 0.93 (Figures 2J–K). These results highlight that the

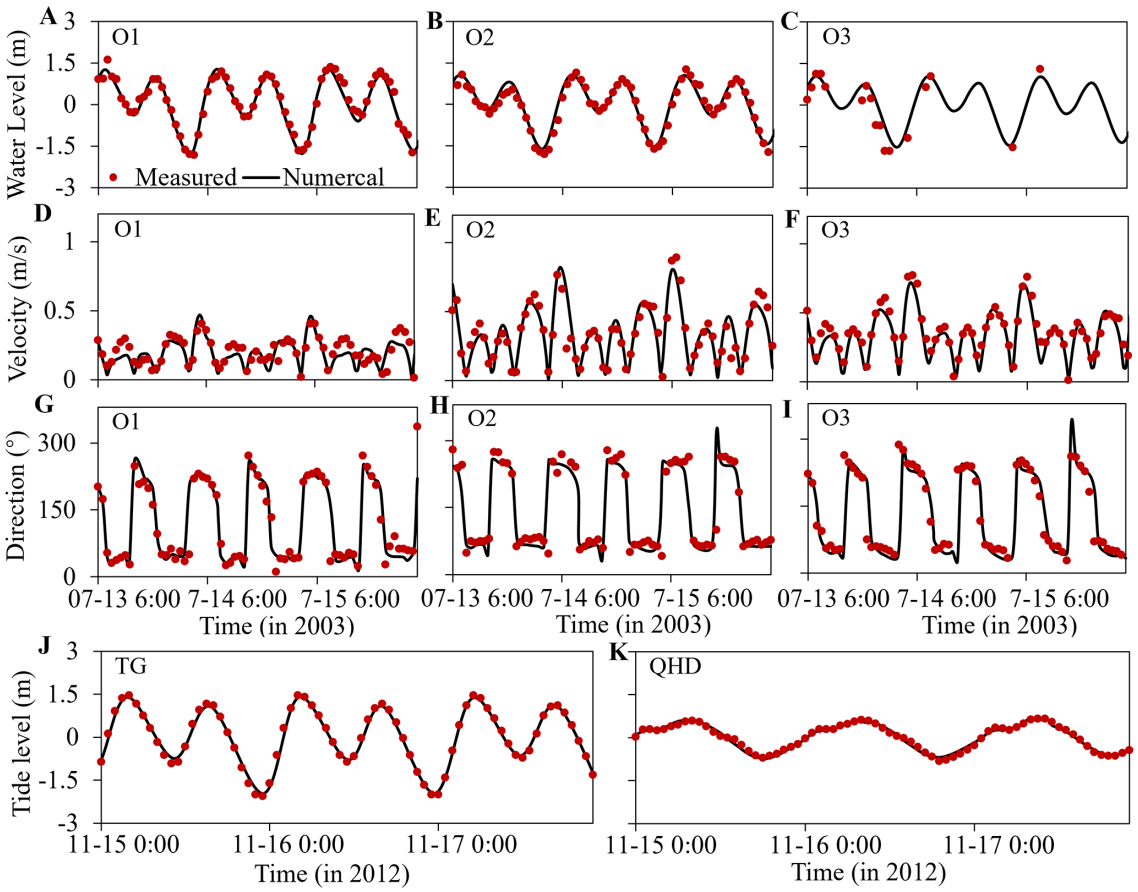

FIGURE 2
Comparison between measured and simulated values. **(A–C)** Water levels. **(D–F)** Flow velocities. **(G–I)** Flow directions. **(J–K)** Tide levels.

present hydrodynamic model can be used to simulate the tidal propagation and fluctuation processes in the BS.

2.3.2 Simulation scenarios

The historical coastline conditions were simulated using topographic survey data circa 1855, 1962, 1981, and 2003, spanning over a century. To address the data gap between 1855 and 1962, three hypothetical coastlines (H1-H3; see Table 1) were set to ensure continuity in the simulations and to capture long-term trend.

TABLE 1 Simulation scenarios.

Historical scenarios			Future scenarios		
Run	Area/ km^2	Time/a	Run	Area/ km^2	Time/a
1855	-2410	-148	R1	244	23
H1	-1942	-120	R2	608	44
H2	-1358	-85	R3	1035	72
H3	-923	-59	R4	1571	107
1962	-621	-41			
1981	-191	-22			
2003	0	0			

For future projections, the morphological evolution of the YRD is assumed to be primarily driven by fluvial sediment deposition (Syvitski and Saito, 2007). Based on the measured sediment load data and established land area data from 1959 to 2015 (Figure 3A), a linear regression function was established to describe the relationship between the cumulative delta land accretion area and riverine sediment supply:

$$\sum A = 1.92\sum W_s - 29.45, R^2 = 0.89 \quad (3)$$

where $\sum A$ is cumulative land accretion area of the delta (km^2), $\sum W_s$ is cumulative sediment load (10^8 t). Equation 3 reveals a strong correlation between delta land area and sediment load (Figure 3B). Although sediment delivery to the delta has declined in recent decades due to soil conservation and dam construction in the YR basin, the low sediment load may not be sustained over a long time due to the cyclical nature of climate change and the limited retention capacity of sediment trapping projects upstream (Kong et al., 2016; Wang et al., 2016; Guo et al., 2021). Existing studies has projected future sediment discharge of the YR to range between 0.4 and 1.0 Gt/a (YREC, 2018; Dang et al., 2020; Liu et al., 2024).To reflect this potential variability, the historical sediment series from 1979 to 1985 was adopted and repeated to cover the

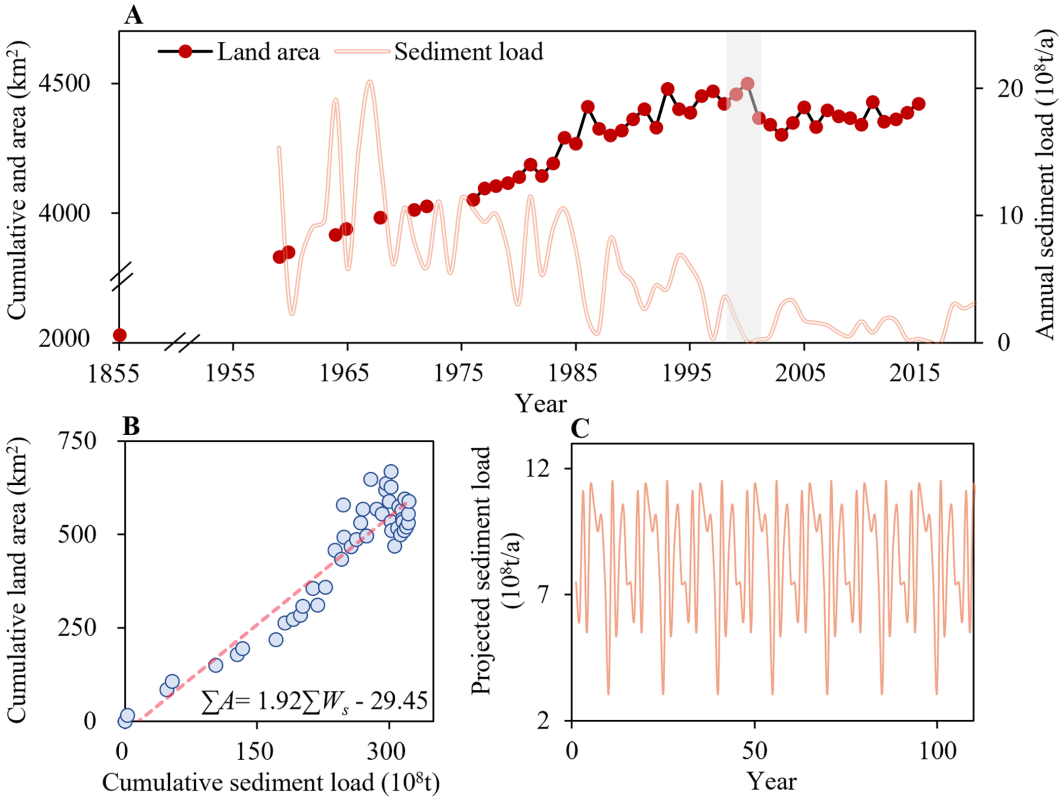

FIGURE 3
Relationship between delta land area and riverine sediment supply. **(A)** Land area changes of the YRD from 1855 to 2015, and annual sediment input from 1959 to 2020. **(B)** Relationship between the cumulative land area and the cumulative sediment load during 1959-2015. **(C)** Future projection of riverine sediment supply.

century-scale simulation period, yielding a multi-year average sediment load of 0.8 Gt/a, with annual values ranging from 0.3 to 1.1 Gt/a (Figure 3C). Based on this dataset, four future scenarios (R1–R4; see Table 1) were developed using Equation 3. The YRD is projected to expand by 1571 km² over the next 107 years. The corresponding shoreline configurations are illustrated in Figure 1B. Rather than predicting a deterministic future state, the projected scenarios enable the exploration of potential feedbacks between delta and adjacent sea in the long term. To isolate the effects of delta coastline changes, this study excludes other anthropogenic modifications in the coastline, such as land reclamation or navigation channel construction.

2.3.3 Data analysis

The tidal flux refers to the volume of tidal water that passes through a section during flood and ebb of the tide. It is calculated based on the Equation 4 (Zhang et al., 2016):

$$W = \int_{t_1}^{t_2} v_t(z_t + h)Bdt \tag{4}$$

where v_t (m/s) is the depth averaged flow velocity, z_t (m) is the free surface variation, h (m) is the water depth, B(m) is the width of the section, t_1 and t_2 are the start and end times of the high tide or low tide cycle, respectively.

Tidal currents act as the persistent hydrodynamic driver shaping the long-term morphological and ecological processes in deltaic systems (Hoitink et al., 2017). To investigate how changes in tidal dynamics may affect the sediment transport process in the estuary, an indicator is introduced to quantify the offshore sediment transport capacity driven by tidal currents. It can be expressed as $Q_s = Q \cdot S$, where $Q = v_t \cdot h$ is the water discharge and $S \sim v_t^2/gh$ is the depth averaged sediment concentration (Yalin, 1977). Then the relationship between the sediment transport capacity and tidal currents can be formulated as: $Q_s \sim v_t^3$. Accordingly, the indicator for the tidal sediment transport capacity (T_s) over a period of t_n can be expressed as Equation 5

$$T_s = \int_0^{t_n} v_t^3 dt/t_n \tag{5}$$

In this study, T_s is calculated as the two-month average value. Since the transport of contaminants and other masses also depends on tidal currents and turbulence, variation in T_s can also be used as a proxy to reflect potential shifts in other transport processes such as pollutant dispersion.

2.4 Theoretical model

To investigate how tide propagates in the bay under the influence of delta expansion, a theoretical model is established. The bay is idealized as a system with a constant width and water depth. Under the small-amplitude and Boussinesq assumptions, and neglecting the Coriolis force, conservation of mass and momentum equations are as Equations 6, 7

$$\frac{\partial Q}{\partial x} + b\frac{\partial \eta}{\partial t} = 0 \tag{6}$$

$$\frac{\partial Q}{\partial t} + \frac{\partial}{\partial x}\left(\frac{Q^2}{A}\right) + gA\frac{\partial \eta}{\partial x} + bF = 0 \tag{7}$$

where $Q = bhu$ is the tidal discharge, b is the width, u is depth averaged velocity, h is water depth, A is the cross-sectional area, η is the water level, g is gravity, $F \sim C_d u|u|$ is the frictional resistance, and C_d is drag coefficient. In the absence of convective acceleration and friction, conservation of mass and momentum equations are as Equation 8

$$A_\star = \frac{\eta_x}{\eta_{x=L}} = \frac{\cos(2\pi/\lambda)x}{\cos(2\pi/\lambda)L} \tag{8}$$

where L is the length of the basin, λ is the tidal wavelength. Further incorporating the friction into the analysis, the amplification ($A_\star$) with friction which has been linearized (Talke and Jay, 2020) as Equations 9-11

$$A_\star = \sqrt{2}\left(\cosh\left(\frac{4\pi L}{\lambda_0}\sigma\right) + \cos\left(\frac{4\pi L}{\lambda_0}\beta\right)\right)^{-1/2} \tag{9}$$

$$\beta = \sqrt{1/2 + 1/2\sqrt{1 + (r/\omega)^2}} \tag{10}$$

$$\sigma = \sqrt{-1/2 + 1/2\sqrt{1 + (r/\omega)^2}} \tag{11}$$

where $\lambda_0 = T\sqrt{gh}$ is the tidal wavelength, $\omega = 2\pi/T$ is angular frequency, $r = 3\pi C_d U/8h$ is the linearized friction coefficient, U is the velocity.

3 Results and discussion

3.1 Tidal responses in the entire Bohai Sea

To investigate the overall impact of the delta expansion on the tidal regime in the BS, tidal flux during spring and neap tides were quantified across four profiles (P1-P4, as shown in Figure 1C). The temporal variations of tidal flux in each profile are illustrated in Figure 4, expressed as relative changes compared to the 2003 value. With the continuous advancement of the YRD coastline since 1855, tidal flux in the major bays exhibited an increasing trend. However, this trend is projected to reverse under future scenarios. The most significant changes occur in the LZB. As the delta coastline continues to advance after 2003, tidal flux is projected to rise by 6-10% in the initial decades, reaching its maximum under scenario R2. It subsequently begins to decline, with the largest reduction of 8.9% under scenario R4 relative to the 2003 levels. In the BHB, tidal flux reached the peak in 1981, and has since shown a decrease, with a maximum projected reduction of 11.5% under scenario R4. Similarly, the expansion of the delta after 2003 leads to a gradual decline in tidal flux in the LDB, with a maximum reduction of 6%. Tidal flux through the Bohai Strait under future scenarios also

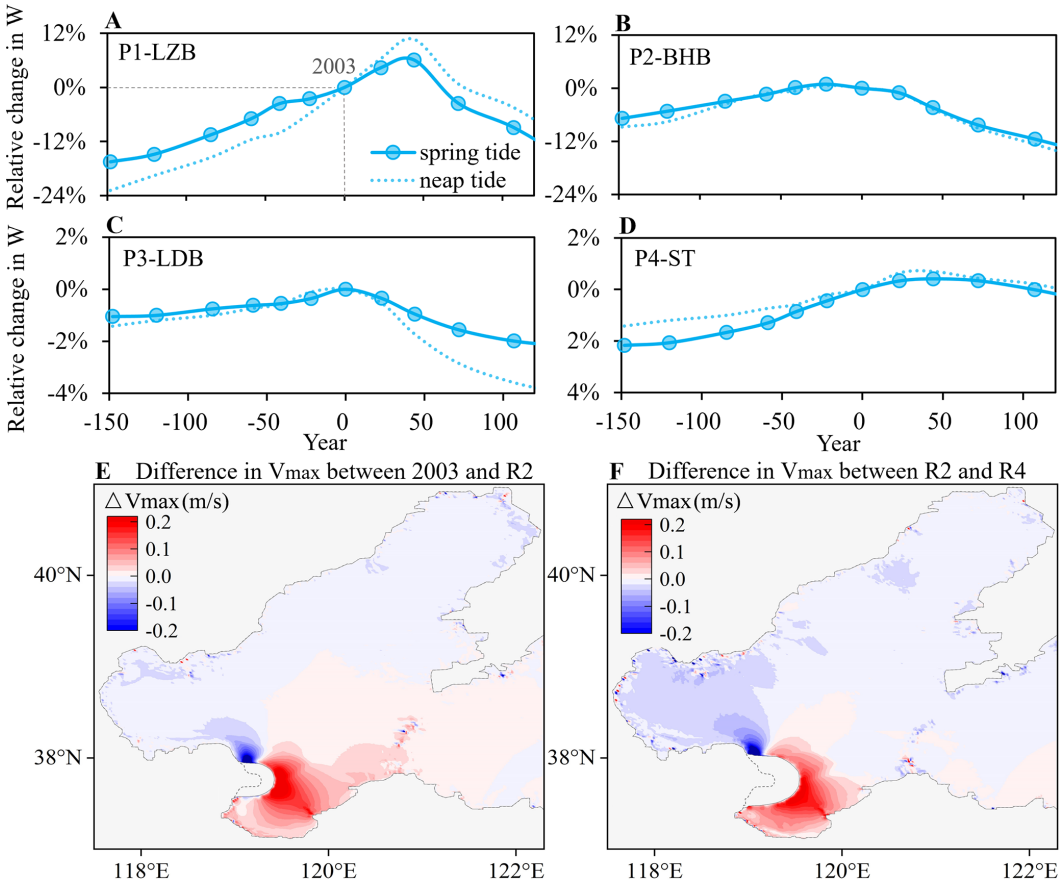

FIGURE 4
Tidal dynamic changes in the BS. **(A)** Relative change in tidal flux across P1-Laizhou Bay (LZB), **(B)** P2-Bohai Bay (BHB), **(C)** P3-Liaodong Bay (LDB), **(D)** P4-Bohai Strait (ST); Tidal flux changes are expressed as percentages relative to the 2003 baseline. **(E)** Difference in maximum tidal flow velocity between 2003 and R2; **(F)** Difference in maximum tidal flow velocity between R2 and R4; The dashed line indicates the 2003 coastline.

exhibits fluctuations, with a reduction of approximately 1%. Overall, the bays in the BS exhibit similar trends in tidal flux variation, with an initial increase followed by a decline. The LZB and BHB, which are adjacent to the YRD and have relatively smaller basin sizes, experience more pronounced variations. In contrast, the LDB, located farther from the delta and occupying a larger area, shows smaller fluctuations in tidal flux.

The spatial distribution of changes in maximum tidal flow velocity (V_{max}) under different delta coastline conditions during spring tides are shown in Figures 4E, F. Relative to 2003, changes in V_{max} under scenario R2 (Figure 4E) exhibit spatial inconsistency, ranging from -0.24 to 0.29 m/s. In the LZB, V_{max} shows a general increasing trend, with the greatest increase reaching up to 0.29 m/s. In contrast, both the BHB and LDB experience decline in V_{max}, with maximum reductions of 0.31 and 0.06 m/s, respectively. A slight increase is observed in the Bohai Strait, with the maximum increase of 0.04 m/s. The difference between scenarios R2 and R4 (Figure 4F) suggests that regions with enhanced flow velocities become spatially confined. While the LZB continues to exhibit increasing V_{max}, with a maximum increase of 0.25 m/s, most other regions of the BS experience further decline, with reductions of up to 0.37 m/s. The largest decrease occurs along the western margin of the YRD. These results indicate that the continued expansion of the delta induces a widespread reduction in tidal flow velocities throughout the BS, including the BHB, LDB and the central area, consistent with the changes in tidal flux. Conversely, the LZB experiences sustained intensification of tidal flow velocities. This localized enhancement is primarily attributed to the morphological shrinkage of the bay, which amplifies local hydrodynamics by concentrating flow within a reduced spatial domain (Hallock et al., 2003). Nevertheless, despite the amplified velocities, the concurrent reduction in bay area ultimately results in a net decrease in tidal flux through the LZB (Figure 4A).

3.2 Tidal dynamics around the delta

Tidal dynamics play a crucial role in controlling sediment deposition and transport processes in the delta, and have also been altered by the delta expansion. Figure 5 illustrates the spatial evolution of tidal sediment transport capacity (T_s) in response to historical and projected shoreline changes. During the initial stage in 1855, when the delta shoreline exhibited a smooth configuration, T_s in the estuarine region remained generally low (Figure 5A). The

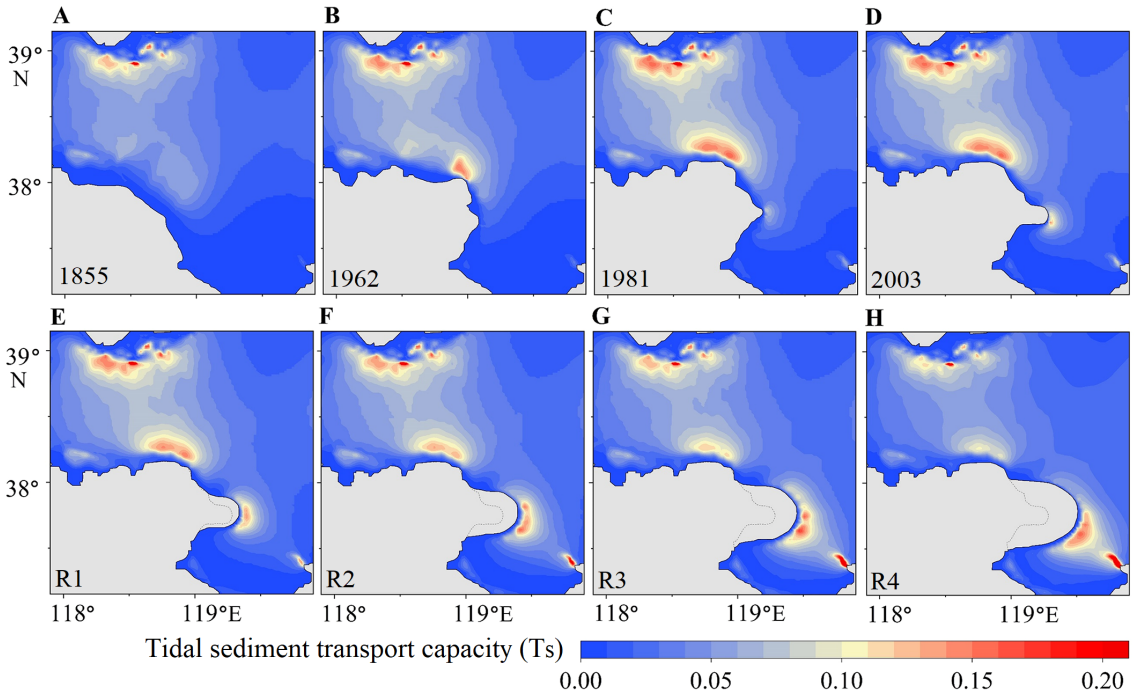

FIGURE 5
Distribution of tidal sediment transport capacity *Ts* around the YRD during different periods. **(A)** 1855; **(B)** 1962; **(C)** 1981; **(D)** 2003; **(E)** R1; **(F)** R2; **(G)** R3; **(H)** R4. The dashed line indicates the 2003 coastline.

subsequent formation of distinct deltaic lobes through sediment deposition created morphological protrusions that modified local hydrodynamic conditions. These geomorphic changes accelerated tidal currents and enhanced T_s near the deltaic lobes. Specifically, the diversion of the deltaic river into the SXG course led to the formation of a new delta lobe by 1962, inducing localized increase in T_s nearshore (Figure 5B). This effect of coastline advancement became more pronounced by 1982, when the shoreline in the northern delta extended seaward by approximately 20 km due to the formation of the DKH lobe, resulting in markedly enhanced T_s along the northern delta front (Figure 5C). Subsequently, the evolution of the QSG lobe by 2003 resulted in a new center of high T_s in the southern delta front (Figure 5D). The tidal dynamics near the DKH lobe remain stronger than the QSG lobe, consistent with observed records (Wang and Liang, 2000).

Under future scenarios (Figures 5E–H), the continuous seaward progradation of the QSG lobe is projected to further intensify T_s near the active river mouth. In contrast, abandoned lobes in the northern delta exhibit a continuous decline in T_s, despite no additional shoreline modification being imposed on those areas. This spatial divergence highlights the non-uniform tidal responses to deltaic evolution, where modifications to one segment of the shoreline can influence tidal dynamics throughout the system. Additionally, while the use of different bathymetry data sources may introduce local discrepancies in tidal magnitude, the tidal evolution patterns observed in this study can be supported by previous studies. Specifically, Bai et al. (2019) simulated flow patterns near the YRD over the past 60 years, demonstrating high-flow-velocity zones closely related to the formation of sand spits in the river mouth; Zhan et al. (2020) indicated that tidal currents off the active delta lobe increased significantly with the progradation of the river mouth since 1976. Similarly, Wang et al. (2015a) revealed the strong tidal current areas shifted from the abandoned to the active river mouth after 1996, with increased flow velocities near the active mouth and a decline near the abandoned lobe. These studies can support the spatial divergence and changing trends captured in this study, that further highlight the feedback between deltaic morphological evolution and tidal dynamics.

3.3 Mechanism of the tidal responses

Here, the propagation of M_2 tide, the dominant tidal constituent in the BS, is investigated by the theoretical model. Figure 6 illustrates the variation of amplification as a function of normalized length (L/λ_0) and friction (r/ω) in the idealized bay. Resonance within the basin is identified at the peaks of the amplification lines. Changes in bay length make the basin approach or move away from the resonance. For basins with a length below the resonant frequency, tidal amplification increases with basin length. Conversely, for systems above this threshold, increasing length would decrease the amplification. The approximate positions of the historical and current YRD within this parameter space of M_2 constitute are shown in Figure 6. Since 1855, expansion of the YRD into the BS has effectively shortened the tidal basin, thereby moving the system closer to resonance. However, the current YRD appears to lie near the threshold point. Further seaward expansion of the delta might shift the

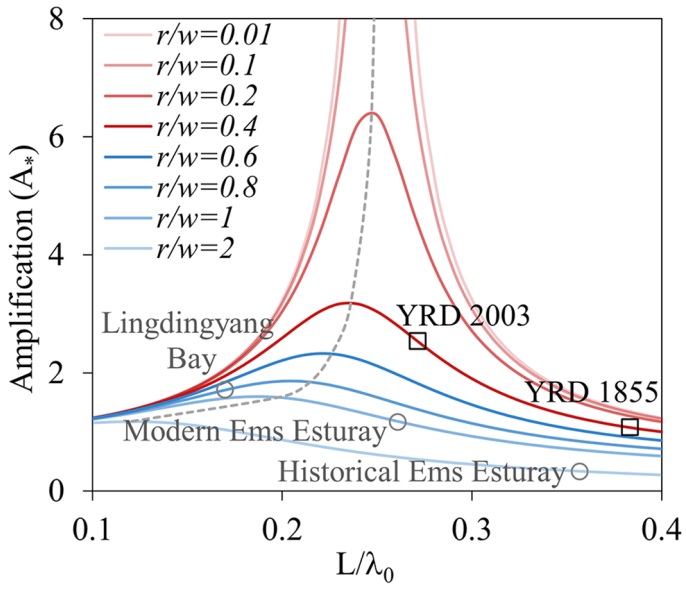

FIGURE 6
Amplification of tide magnitude (M_2 constitute). r/ω indicates friction condition. L/λ_0 is the normalized length. Squares: the approximate locations of YRD in this parameter space. Circles: the approximate locations of other real systems.

system beyond the resonant state, resulting in a gradual decrease of the tidal amplification. It indicates the nonlinear relationship between tidal dynamics and delta coastline evolution, consistent with the numerical simulations. Furthermore, beyond delta evolution, large-scale land reclamation also modifies the shoreline and constrains the bay geometry, producing impacts on tides. Zhu et al. (2018); Liu et al. (2023a), and Wu et al. (2023b) suggested that the land reclamation reduced tidal currents and tidal flux within the BS, leading to increase in residence time and decrease in water exchange capacity. Similar patterns have been observed in other estuary systems. In China's Lingdingyang Bay, large-scale land reclamation projects have reduced tidal flux and weakened tidal currents (Chu et al., 2022). In contrast, the Ems Estuary of Germany has experienced enhanced tidal dynamics due to similar interventions (Chernetsky et al., 2010). These divergent responses are primarily driven by differences in their resonance state (Figure 6). While this geometric control is fundamental, resonance in more physically realistic systems, however, is influenced by additional factors including depth variations, width convergence and bottom friction (Ralston et al., 2019; Larson et al., 2020; Gao et al., 2024). Changes in depth and width influence the progradation speed of tidal waves and frictional damping, thereby altering the resonant frequency and maximum amplification (Roos and Schuttelaars, 2011; Ensing et al., 2015). As shown in Figure 6, changes in water depth (h) could modify both friction (r/ω) and tidal wavelength (λ_0), and increased friction (r/ω) reduces the maximum amplification. Despite the simplifications used in the model, it still provides valuable insights into how the resonance might be altered by geometry changes (Talke and Jay, 2020), as it captures the dominant tidal constituent and characteristic scales of the BS.

Furthermore, the simulation results reveal an intensification of local tidal dynamics near the active deltaic lobe and in the adjacent LZB. As the active delta lobe shoreline protrudes seaward, the convex shoreline geometry accelerates tidal currents in the nearshore regions. This process is analogous to flow around a bluff body, where fluid passing a body with a broad cross-section experiences flow separation and local acceleration due to pressure gradients and streamline deflection (Bearman, 1984). Similarly, the advancing delta lobe acts as a bluff obstacle in the tidal flow field, enhancing nearshore velocities.

3.4 Implications for coastal sustainability

The YRD evolves under changing tidal conditions. The YR has discharged into a shallow embayment following the shift of the river mouth from the DKH to QSG course in 1976. Weak tidal currents near the river mouth have favored sediment accumulation on the delta plain and accelerated the infilling of the shallow embayment for land building (Zhang et al., 2018). Previous studies examined that over 70% of the sediment delivered by the YR was deposited within the nearshore region (Zhou et al., 2020), exceeding the 50–60% deposition rate observed at the abandoned lobes (Dong, 1997), where the tidal currents were stronger. Tidal dynamics and sediment transport capacity near the active QSG lobe are projected to enhance with the continued progradation of the river mouth. However, it should be noted that such intensification depends on the elongation of the river mouth, which could elevate the base level of the perched lower YR and increase the risk of overbank flooding (Shi et al., 2019; Zheng et al., 2019). Meanwhile, tidal dynamics near the abandoned DKH lobe weakens

with the expansion of the active lobe. There is an alternative flow path within the DKH lobe, which could potentially replace the current QSG course or serve as a flood diversion channel (Qian et al., 2023). However, the decline in tidal currents might hinder sediment dispersal and promote further sedimentation in the standby river mouth. This trend poses challenges to the long-term morphological stability of the delta and may affect its resilience to future changes.

Furthermore, the progressive seaward expansion of the YRD acts as a protruding boundary that disrupts the propagation and reflection of tidal waves. This morphological evolution is projected to diminish tidal currents and reduce tidal flux across the major bays. The BHB, where major ports like Caofeidian and Huanghua are located, shows a significant decline in tidal currents. The weakened tidal dynamics could reduce natural sediment flushing and dispersal in navigation channels (Song et al., 2013; Huang et al., 2023), accelerating siltation in port basins and increasing reliance on dredging operations, thus elevating maintenance costs (Fuller et al., 2024; Deng et al., 2025). In addition, diminished tidal dynamics could increase the water residence time within the basin (Wisha et al., 2018; Wu et al., 2023b). This prolonged retention directly elevates the risk of eutrophication by allowing nutrients from riverine inputs and coastal activities to accumulate (Mundaca et al., 2025) and fueling persistent phytoplankton blooms (Ouyang et al., 2023), including harmful algal blooms (Song et al., 2016). Meanwhile, the accumulation of pollutants such as heavy metals and microplastics might also be exacerbated, posing chronic threats to marine organisms and ecosystem health (Li et al., 2018). Moreover, the loss of tidal mixing could promote stratification of the water column and reduce vertical exchange of oxygen, increasing the likelihood of hypoxic or even anoxic conditions in bottom waters (Zhang et al., 2022a; Wu et al., 2025). The hypoxic emerges as a major threat to marine biodiversity, leading to mass death of benthic organisms and disrupting the structure and function of marine ecosystems (Rakocinski et al., 2023; Thompson et al., 2023). Reduced growth and reproduction linked to poor water conditions also lead to substantial declines in fishery yields and economic losses for coastal communities (Huang et al., 2010; Liu et al., 2023b). Given the limited environmental capacity and ecological vulnerability of the BS, tidal weakening induced by delta expansion warrants attention in coastal management.

3.5 Uncertainty analysis and outlooks

To evaluate the robustness of the simulation results, an uncertainty analysis was conducted focusing on key parameters including friction (quantified by Manning coefficients) and grid resolution. Manning coefficients were varied from 0.014 to 0.020 relative to the baseline value of 0.0165. Water levels and tidal flow velocities during spring tide were analyzed at three representative sites for comparison (LZ, BH, and LD; see Figure 1C). Variations in Manning coefficients primarily affected the magnitude of water levels and tidal currents, with increased friction leading to reduced tidal dynamics (Figures 7A–F). Meanwhile, minimal phase shifts were observed, indicating little impact on the simulated trend in tidal responses. To examine spatial resolution sensitivity, simulations were performed using both the original 1.5 km grid

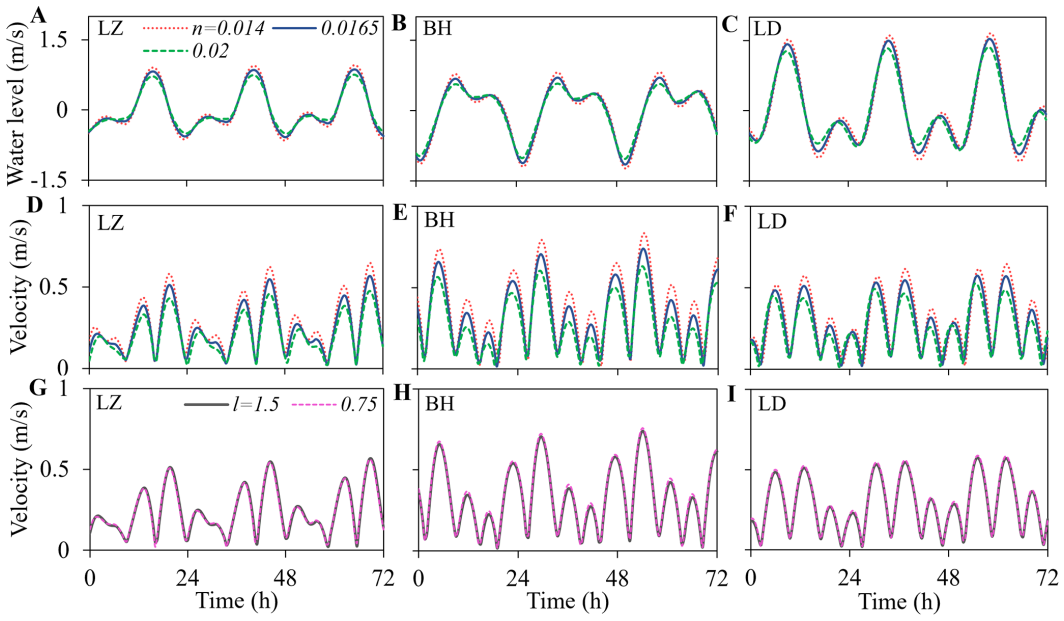

FIGURE 7
Water levels and flow velocities under parameter sensitivity analysis. **(A–C)** Water levels, and **(D–F)** flow velocities under various Manning coefficients (*n*). **(G–I)** Flow velocities under various grid resolution refinements. *l* denotes the grid resolution in longitudinal and latitudinal directions. LZ, BH, and LD are measurement points located in the LZB, BHB and LDB, respectively.

and a refined 0.75 km grid. The refined mesh resulted in only minor differences in tidal currents, with the RMSE values for simulated velocities below 0.015 m/s (Figures 7G–I). These results suggest that the baseline grid resolution is adequate for capturing the basin-scale tidal dynamics.

This study estimates the tidal evolution across the BS to long-term expansion of the YRD. While the findings offer valuable insights into geometry-tidal feedbacks and their implications for coastal sustainability, certain limitations regarding the method should be acknowledged. First, the use of static shorelines neglects short-term morphological changes, which may affect nearshore hydrodynamics at finer spatial scales (Cao et al., 2023). Second, the analysis focuses solely on tidal dynamics, whereas other processes such as wind-waves, especially during winter storms, could temporarily enhance water levels and currents in estuaries (Zhao et al., 2025). In addition, the two-dimensional model does not account for density-stratification effects which may influence sediment deposition processes in the river mouth during flood events (Wu et al., 2023a). These factors operate at distinct spatiotemporal scales and are worth being considered in future work to achieve a more comprehensive understanding of coupled estuarine dynamics.

4 Conclusions

In this study, the tidal responses across the BS throughout the historical and projected expansion of the YRD were investigated using a large-scale hydrodynamic model. The mechanisms driving the changing tides were explored based on the theoretical analysis. In addition, the potential implications for the coastal region were analyzed. The findings reveal that the continuous seaward expansion of the YRD has altered the tidal resonance states of the BS, inducing nonlinear variations in tidal dynamics. Historical delta progradation since 1855 has led to enhanced tidal currents and flux across the major bays. However, future expansion of the delta is projected to reduce tidal fluxes and flow velocities across most regions of the BS in the coming decades. Local tidal currents and sediment transport capacity are projected to increase around the active QSG lobe due to the elongated river mouth, at the cost of the base-level rise of the perched YR. Conversely, the abandoned lobes experience decreased tidal dynamics as the active lobe progrades seaward, potentially hindering sediment dispersal in the standby river mouth. The sustained seaward expansion of the YRD raises concerns regarding coastal sustainability. The projected reduction in tidal currents and flux in the BS may diminish water exchange capacity and tidal mixing, thereby increasing the risk of water quality deterioration and ecological degradation. These findings highlight the critical need to incorporate tidal feedbacks into future coastal planning and delta management to safeguard the morphological and ecological stability of the coupled system.

Data availability statement

The original contributions presented in the study are included in the article/supplementary material.Further inquiries can be directed to the corresponding author/s.

Author contributions

JS: Writing – original draft, Investigation, Visualization, Data curation, Writing – review & editing, Methodology. MZ: Funding acquisition, Data curation, Writing – review & editing, Methodology. JZ: Project administration, Conceptualization, Supervision, Writing – review & editing.

Funding

The author(s) declare that financial support was received for the research and/or publication of this article. This work is supported by Key Technologies Research and Development Program (2022YFC3202701).

Conflict of interest

The authors declare that the research was conducted in the absence of any commercial or financial relationships that could be construed as a potential conflict of interest.

Generative AI statement

The author(s) declare that no Generative AI was used in the creation of this manuscript.

Publisher's note

References

Ayyappan, K., Thiruvenkatasamy, K., Balu, R., Devendrapandi, G., Kadaikunnan, S., and Ayyamperumal, R. (2024). Numerical model study on stability of a micro-tidal inlet at Muttukadu along the east coast of Bay of Bengal. *Environ. Res.* 248, 1–13. doi: 10.1016/j.envres.2024.118304

Bai, Y., Xie, Q., and Xu, H. (2019). The evolution process of tidal characteristics in the last 60 years of the Yellow River Estuary. *Mar. Sci. Bull. (Beijing)* 38, 141–149. doi: 10.11840/j.issn.1001-6392.2019.02.003

Bearman, P. W. (1984). Vortex shedding from oscillating bluff-bodies. *Annu. Rev. Fluid Mechanics* 16, 195–222. doi: 10.1146/annurev.fl.16.010184.001211

Bi, N., Wang, H., Wu, X., Saito, Y., Xu, C., and Yang, Z. (2021). Phase change in evolution of the modern Huanghe (Yellow River) Delta: Process, pattern, and mechanisms. *Mar. Geology* 437, 1–15. doi: 10.1016/j.margeo.2021.106516

Cao, Y., Wang, Q., Zhan, C., Li, R., Qian, Z. F., Wang, L. S., et al. (2023). Evolution of tidal flats in the Yellow River Qingshuigou sub-delta: spatiotemporal analysis and mechanistic changes, (1996-2021). *Front. Mar. Sci.* 10. doi: 10.3389/fmars.2023.1286188

Chernetsky, A. S., Schuttelaars, H. M., and Talke, S. A. (2010). The effect of tidal asymmetry and temporal settling lag on sediment trapping in tidal estuaries. *Ocean Dynamics* 60, 1219–1241. doi: 10.1007/s10236-010-0329-8

Chu, N., Yao, P., Ou, S., Wang, H., Yang, H., and Yang, Q. (2022). Response of tidal dynamics to successive land reclamation in the Lingding Bay over the last century. *Coast. Eng.* 173, 1–15. doi: 10.1016/j.coastaleng.2022.104095

Dang, S. Z., Liu, X. Y., Yin, H. J., and Guo, X. W. (2020). Prediction of sediment yield in the middle reaches of the yellow river basin under extreme precipitation. *Front. Earth Sci.* 8. doi: 10.3389/feart.2020.542686

Deng, X. L., Wang, Z. F., and Ma, X. (2025). Impact of silted coastal port engineering construction on marine dynamic environment: A case study of binhai port. *J. Mar. Sci. Eng.* 13, 1–26. doi: 10.3390/jmse13030494

Dong, N. (1997). The deposit and diffuse of the Yellow River sediment into the sea. *Ocean Eng.* 15, 59–59. doi: 10.16483/j.issn.1005-9865.1997.02.008

Egbert, G. D., and Erofeeva, S. Y. (2002). Efficient inverse Modeling of barotropic ocean tides. *J. Atmospheric Oceanic Technol.* 19, 183–204. doi: 10.1175/1520-0426(2002)019<0183:Eimobo>2.0.Co;2

Ensing, E., de Swart, H. E., and Schuttelaars, H. M. (2015). Sensitivity of tidal motion in well-mixed estuaries to cross-sectional shape, deepening, and sea level rise. *Ocean Dynamics* 65, 933–950. doi: 10.1007/s10236-015-0844-8

Fan, Y. S., Chen, S. L., Zhao, B., Yu, S. B., Ji, H. Y., and Jiang, C. (2018). Monitoring tidal flat dynamics affected by human activities along an eroded coast in the Yellow River Delta, China. *Environ. Monit. Assess.* 190, 1–17. doi: 10.1007/s10661-018-6747-7

Fu, Y. T., Chen, S. L., Ji, H. Y., Fan, Y. S., and Li, P. (2021). The modern Yellow River Delta in transition: Causes and implications. *Mar. Geology* 436, 1–14. doi: 10.1016/j.margeo.2021.106476

Fuller, W. P., Wagner, R. J., and Lewis, R. E. (2024). US hydrodynamic dredging challenges and opportunities. *Transportation Res. Rec.* 2678, 487–500. doi: 10.1177/03611981231207849

Ganti, V., Chu, Z. X., Lamb, M. P., Nittrouer, J. A., and Parker, G. (2014). Testing morphodynamic controls on the location and frequency of river avulsions on fans versus deltas: Huanghe (Yellow River), China. *Geophysical Res. Lett.* 41, 7882–7890. doi: 10.1002/2014gl061918

Gao, J. L., Hou, L. H., Liu, Y. Y., and Shi, H. B. (2024). Influences of bragg reflection on harbor resonance triggered by irregular wave groups. *Ocean Eng.* 305, 1–22. doi: 10.1016/j.oceaneng.2024.117941

Gao, J. L., Ma, X. Z., Dong, G. H., Chen, H. Z., Liu, Q., and Zang, J. (2021). Investigation on the effects of Bragg reflection on harbor oscillations. *Coast. Eng.* 170, 1–17. doi: 10.1016/j.coastaleng.2021.103977

Gao, J. L., Ma, X. Z., Zang, J., Dong, G. H., Ma, X. J., Zhu, Y. Z., et al. (2020). Numerical investigation of harbor oscillations induced by focused transient wave groups. *Coast. Eng.* 158, 1–17. doi: 10.1016/j.coastaleng.2020.103670

Guo, W. Z., Wang, W. L., Xu, Q., Hu, J. J., and Zhu, L. L. (2021). Distribution, failure risk and reinforcement necessity of check-dams on the Loess Plateau: a review. *J. Mountain Sci.* 18, 499–509. doi: 10.1007/s11629-020-6090-7

Hallock, Z. R., Pistek, P., Book, J. W., Miller, J. L., Shay, L. K., and Perkins, H. T. (2003). A description of tides near the Chesapeake Bay entrance using in *situ* data with an adjoint model. *J. Geophysical Research-Oceans* 108, 1–9. doi: 10.1029/2001jc000820

Hoitink, A. J. F., Wang, Z. B., Vermeulen, B., Huismans, Y., and Kastner, K. (2017). Tidal controls on river delta morphology. *Nat. Geosci.* 10, 637–645. doi: 10.1038/ngeo3000

Huang, L., Smith, M. D., and Craig, J. K. (2010). Quantifying the economic effects of hypoxia on a fishery for brown shrimp farfantepenaeus aztecus. *Mar. Coast. Fisheries* 2, 232–248. doi: 10.1577/c09-048.1

Huang, Z., Xu, H. J., Bai, Y. C., Shi, F. S., and Wen, Z. C. (2023). Coastline changes and tidal current responses due to the large-scale reclamations in the Bohai Bay. *J. Oceanology Limnology* 41, 2045–2059. doi: 10.1007/s00343-022-2235-6

Ji, H., Chen, S., Pan, S., Xu, C., Tian, Y., Li, P., et al. (2022). Fluvial sediment source to sink transfer at the Yellow River Delta: Quantifications, causes, and environmental impacts. *J. Hydrology* 608, 1–13. doi: 10.1016/j.jhydrol.2022.127622

Ji, H., Pan, S., and Chen, S. (2020). Impact of river discharge on hydrodynamics and sedimentary processes at Yellow River Delta. *Mar. Geology* 425, 1–14. doi: 10.1016/j.margeo.2020.106210

Jiang, C., Pan, S., and Chen, S. (2017). Recent morphological changes of the Yellow River (Huanghe) submerged delta: Causes and environmental implications. *Geomorphology* 293, 93–107. doi: 10.1016/j.geomorph.2017.04.036

Juarez, B., Alegria-Arzaburu, A. R. D., and Walther, J. G. (2025). Tidal amplification and shallow water tides in a mixed semidiurnal coastal lagoon. *Continental Shelf Res.* 289, 1–14. doi: 10.1016/j.csr.2025.105468

Kong, D., Miao, C., Borthwick, A. G. L., Duan, Q., Liu, H., Sun, Q., et al. (2015). Evolution of the Yellow River Delta and its relationship with runoff and sediment load from 1983 to 2011. *J. Hydrology* 520, 157–167. doi: 10.1016/j.jhydrol.2014.09.038

Kong, D. X., Miao, C. Y., Wu, J. W., and Duan, Q. Y. (2016). Impact assessment of climate change and human activities on net runoff in the Yellow River Basin from 1951 to 2012. *Ecol. Eng.* 91, 566–573. doi: 10.1016/j.ecoleng.2016.02.023

Larson, M., Nunes, A., and Tanaka, H. (2020). Semi-analytic model of tidal-induced inlet flow and morphological evolution. *Coast. Eng.* 155, 103581. doi: 10.1016/j.coastaleng.2019.103581

Li, Y. F., Wolanski, E., Dai, Z. F., Lambrechts, J., Tang, C., and Zhang, H. (2018). Trapping of plastics in semi-enclosed seas: Insights from the Bohai Sea, China. *Mar. pollut. Bull.* 137, 509–517. doi: 10.1016/j.marpolbul.2018.10.038

Liu, L. Y., Yuan, D. K., Li, X., and Mao, Y. T. (2023a). Influence of reclamation on the water exchange in Bohai Bay using trajectory clustering. *Stochastic Environ. Res. Risk Assess.* 37, 3571–3583. doi: 10.1007/s00477-023-02463-8

Liu, S. M., Liang, W., Guo, X., Wu, N., Zhang, W., Shan, X., et al. (2023b). Biogeochemistry-ecosystem-social interactions on the Chinese continental margins. *Oceanologia* 65, 278–296. doi: 10.1016/j.oceano.2022.12.001

Liu, X., Wang, P., and Dang, S. (2024). Variations in water and sediment of the Yellow River: Historical perspectives,current status, and future outlook. *J. Hydraulic Eng.* 55, 1135–1145. doi: 10.13243/j.cnki.slxb.20240433

Lu, J., Zhang, Y., Lv, X., and Shi, H. (2022). The temporal evolution of coastlines in the bohai sea and its impact on hydrodynamics. *Remote Sens.* 14, 1–19. doi: 10.3390/rs14215549

Miao, H., Qiao, L., Zhong, Y., and Li, G. (2022). Evolution of tidal system and material transport off the Huanghe River Delta induced by human activities and natural evolution. *Acta Oceanologica Sin.* 44, 73–86. doi: 10.12284/hyxb2022071

Milliman, J. D., and Syvitski, J. P. (1992). Geomorphic/tectonic control of sediment discharge to the ocean: the importance of small mountainous rivers. *J. Geology* 100, 525–544. doi: 10.1086/629606

Morovati, K., Tian, F. Q., Kummu, M., Shi, L. D., Tudaji, M., Nakhaei, P., et al. (2023). Contributions from climate variation and human activities to flow regime change of Tonle Sap Lake from 2001 to 2020. *J. Hydrology* 616, 1–13. doi: 10.1016/j.jhydrol.2022.128800

Mundaca, V., Echevin, V., Vergara, O. A., Artal, O., and Sepulveda, H. H. (2025). Dynamics of the subtidal transport through the Guafo Mouth connecting the open ocean and the Chilean Inland Sea in southern Chile. *Continental Shelf Res.* 288, 1–11. doi: 10.1016/j.csr.2025.105428

Nienhuis, J. H., Ashton, A. D., Edmonds, D. A., Hoitink, A., Kettner, A. J., Rowland, J. C., et al. (2020). Global-scale human impact on delta morphology has led to net land area gain. *Nature* 577, 514–518. doi: 10.1038/s41586-019-1905-9

Ouyang, W., Wang, R., Ji, K. Y., Liu, X. T., Geng, F., Hao, X., et al. (2023). Phytoplankton biomass dynamics with diffuse terrestrial nutrients pollution discharge into bay. *Chemosphere* 313, 1–10. doi: 10.1016/j.chemosphere.2022.137674

Pan, H. D., Jiao, S. Y., Xu, T. F., Lv, X. Q., and Wei, Z. X. (2022). Investigation of tidal evolution in the Bohai Sea using the combination of satellite altimeter records and numerical models. *Estuar. Coast. Shelf Sci.* 279, 1–13. doi: 10.1016/j.ecss.2022.108140

Passeri, D. L., Hagen, S. C., Medeiros, S. C., and Bilskie, M. V. (2015). Impacts of historic morphology and sea level rise on tidal hydrodynamics in a microtidal estuary (Grand Bay, Mississippi). *Continental Shelf Res.* 111, 150–158. doi: 10.1016/j.csr.2015.08.001

Pelling, H. E., Uehara, K., and Green, J. A. M. (2013). The impact of rapid coastline changes and sea level rise on the tides in the Bohai Sea, China. *J. Geophysical Research-Oceans* 118, 3462–3472. doi: 10.1002/jgrc.20258

Qian, Y., Xu, D., Wang, Q., and Liu, J. (2023). Study on service life of flow paths with using parallel-running mode in two flow paths of Yellow River estuary. *Yellow River* 45, 46–50. doi: 10.3969/j.issn.1000-1379.2023.05.010

Qiao, L., Zhong, Y., Wang, N., Zhao, K., Huang, L., and Wang, Z. (2016). Seasonal transportation and deposition of the suspended sediments in the Bohai Sea and Yellow Sea and the related mechanisms. *Ocean Dynamics* 66, 751–766. doi: 10.1007/s10236-016-0950-2

Rakocinski, C. F., Hendon, J. R., VanderKooy, K. E., Higgs, J. M., Schweiss, V. R., McIntosh, S. C., et al. (2023). Hypoxia interrupts the secondary production service provided by oyster reef macrofauna in mississippi sound, USA. *Estuaries Coasts* 46, 1494–1514. doi: 10.1007/s12237-023-01212-y

Ralston, D. K., Talke, S., Geyer, W. R., Al-Zubaidi, H. A. M., and Sommerfield, C. K. (2019). Bigger tides, less flooding: effects of dredging on barotropic dynamics in a highly modified estuary. *J. Geophysical Research: Oceans* 124, 196–211. doi: 10.1029/2018JC014313

Roos, P. C., and Schuttelaars, H. M. (2011). Influence of topography on tide propagation and amplification in semi-enclosed basins. *Ocean Dynamics* 61, 21–38. doi: 10.1007/s10236-010-0340-0

Shi, C., Zhou, Y., Liu, X., and Chen, X. (2019). River base level change in mouth channel evolution: The case of the Yellow River delta, China. *Catena* 183, 1–10. doi: 10.1016/j.catena.2019.104193

Song, D., Wang, X. H., Cao, Z., and Guan, W. (2013). Suspended sediment transport in the Deepwater Navigation Channel, Yangtze River Estuary, China, in the dry season 20091. Observations over spring and neap tidal cycles. *J. Geophysical. Res.: Oceans* 118, 5555–5567. doi: 10.1002/jgrc.20410

Song, N. Q., Wang, N., Lu, Y., and Zhang, J. R. (2016). Temporal and spatial characteristics of harmful algal blooms in the Bohai Sea during 1952-2014. *Continental Shelf Res.* 122, 77–84. doi: 10.1016/j.csr.2016.04.006

Syvitski, J. P., and Saito, Y. (2007). Morphodynamics of deltas under the influence of humans. *Global Planetary Change* 57, 261–282. doi: 10.1016/j.gloplacha.2006.12.001

Talke, S. A., and Jay, D. A. (2020). Changing tides: The role of natural and anthropogenic factors. *Annual Rev. Mar. Sci.* 12, 121–151. doi: 10.1146/annurev-marine-010419-010727

Tang, G., Feng, D., Wang, F., and Hou, X. (2020). Research on the evolution characteristics of the yellow river delta coastline and its critical values of siltation and erosion. *J. North China Univ. Water Resour. Electric Power (Natural Sci. Edition)* 41, 40–46. doi: 10.19760/j.ncwu.zk.2020074

Tessler, Z. D., Vörösmarty, C. J., Grossberg, M., Gladkova, I., Aizenman, H., Syvitski, J. P. M., et al. (2015). Profiling risk and sustainability in coastal deltas of the world. *Science* 349, 638–643. doi: 10.1126/science.aab3574

Thompson, P. L., Nephin, J., Davies, S. C., Park, A. E., Lyons, D. A., Rooper, C. N., et al. (2023). Groundfish biodiversity change in northeastern Pacific waters under projected warming and deoxygenation. *Philos. Trans. R. Soc. B-Biological Sci.* 378, 1–13. doi: 10.1098/rstb.2022.0191

Tian, K., Wu, Q. M., Liu, P., Hu, W. Y., Huang, B., Shi, B., et al. (2020). Ecological risk assessment of heavy metals in sediments and water from the coastal areas of the Bohai Sea and the Yellow Sea. *Environ. Int.* 136, 1–15. doi: 10.1016/j.envint.2020.105512

Vangelder, A., Vandenberg, J. H., Cheng, G., and Xue, C. T. (1994). Overbank and channelfill deposits of the modern Yellow River Delta. *Sedimentary Geology* 90, 293–305. doi: 10.1016/0037-0738(94)90044-2

Wang, S., Fu, B., Piao, S., Lu, Y., Ciais, P., Feng, X., et al. (2016). Reduced sediment transport in the Yellow River due to anthropogenic changes. *Nat. Geosci.* 9, 38. doi: 10.1038/ngeo2602

Wang, Z., and Huang, S. (1988). Study change of the Yellow River Delta by means of sea charts measured in the recent and the ancient years. *Coast. Eng.* 2, 47–58.

Wang, N., Li, G., Xu, J., Qiao, L., Dada, O. A., and Zhou, C. (2015). The marine dynamics and changing trend off the modern Yellow River mouth. *J. Ocean Univ. China* 14, 433–445. doi: 10.1007/s11802-015-2764-0

Wang, Z. Y., and Liang, Z. Y. (2000). Dynamic characteristics of the Yellow River mouth. *Earth Surface Processes Landforms* 25, 765–782. doi: 10.1002/1096-9837(200007)25:7<765::AID-ESP98>3.0.CO;2-K

Wang, P. T., Wang, Y. C., Wang, Z. C., Gao, Y., Sun, L. N., Li, H. W., et al. (2022). Tsunami free oscillations excited by potential local earthquake sources in Bohai Sea, China. *Ocean Eng.* 266, 1–18. doi: 10.1016/j.oceaneng.2022.112949

Wang, X., Xiao, X., Zou, Z., Chen, B., Ma, J., Dong, J., et al. (2020). Tracking annual changes of coastal tidal flats in China during 1986–2016 through analyses of Landsat images with Google Earth Engine. *Remote Sens. Environ.* 238, 110987. doi: 10.1016/j.rse.2018.11.030

Wang, X., Yan, F., and Su, F. (2021). Changes in coastline and coastal reclamation in the three most developed areas of China 1980-2018. *Ocean Coast. Manage.* 204, 1–12. doi: 10.1016/j.ocecoaman.2021.105542

Wisha, U. J., Al Tanto, T., Pranowo, W. S., and Husrin, S. (2018). Current movement in Benoa Bay water, Bali, Indonesia: Pattern of tidal current changes simulated for the condition before, during, and after reclamation. *Regional Stud. Mar. Sci.* 18, 177–187. doi: 10.1016/j.rsma.2017.10.006

Wu, W. F., Song, C. Y., Chen, Y. C., Zhai, F. G., Liu, Z. Z., Liu, C., et al. (2025). High-frequency dynamics of bottom dissolved oxygen in temperate shelf seas: The joint role of tidal mixing and sediment oxygen demand. *Limnology Oceanography* 70, 1–14. doi: 10.1002/lno.12733

Wu, G., Wang, K., Liang, B., Wu, X., Wang, H., Li, H., et al. (2023a). Modeling the morphological responses of the yellow river delta to the water-sediment regulation scheme: the role of impulsive river floods and density-driven flows. *Water Resour. Res.* 59, 1–22. doi: 10.1029/2022wr033003

Wu, Z., Zhou, C., Wang, P., and Fei, Z. (2023b). Responses of tidal dynamic and water exchange capacity to coastline change in the Bohai Sea, China. *Front. Mar. Sci.* 10. doi: 10.3389/fmars.2023.1118795

Xu, X. G., Chen, Z. X., and Feng, Z. (2019). From natural driving to artificial intervention: Changes of the Yellow River estuary and delta development. *Ocean Coast. Manage.* 174, 63–70. doi: 10.1016/j.ocecoaman.2019.03.009

Yalin, M. S. (1977). *Mechanics of Sediment Transport* (Oxford: Pergaman Press).

YREC (2018). *Special report on variations and the conditions of flow-sediment for the Guxian reservoir, the Yellow River* (Zhengzhou: Yellow River Engineering Consulting Co., Ltd).

Zhan, C., Wang, Q., Cui, B., Zeng, L., Dong, C., Li, X., et al. (2020). The morphodynamic difference in the western and southern coasts of Laizhou Bay: Responses to the Yellow River Estuary evolution in the recent 60 years. *Global Planetary Change* 187, 1–14. doi: 10.1016/j.gloplacha.2020.103138

Zhang, X. D., Lu, Z. Y., Jiang, S. H., Chi, W. Q., Zhu, L. H., Wang, H. M., et al. (2018). The progradation and retrogradation of two newborn Huanghe (Yellow River) Delta lobes and its influencing factors. *Mar. Geology* 400, 38–48. doi: 10.1016/j.margeo.2018.03.006

Zhang, L., Shi, H., Xing, H., Li, P., and Ma, P. (2023). Analysis of the evolution of the Yellow River Delta coastline and the response of the tidal current field. *Front. Mar. Sci.* 10. doi: 10.3389/fmars.2023.1232060

Zhang, M., Townend, I. H., Cai, H., and Zhou, Y. (2016). Seasonal variation of tidal prism and energy in the Changjiang River estuary: a numerical study. *Chin. J. Oceanology Limnology* 34, 219–230. doi: 10.1007/s00343-015-4302-8

Zhang, H. Y., Wei, H., Zhao, L., Zhao, H. D., Guo, S. A., and Zheng, N. (2022a). Seasonal evolution and controlling factors of bottom oxygen depletion in the Bohai Sea. *Mar. pollut. Bull.* 174, 1–11. doi: 10.1016/j.marpolbul.2021.113199

Zhang, W., Xu, Y. J., Guo, L., Lam, N. S. N., Xu, K., Yang, S., et al. (2022b). Comparing the Yangtze and Mississippi River Deltas in the light of coupled natural-human dynamics: Lessons learned and implications for management. *Geomorphology* 399, 1–12. doi: 10.1016/j.geomorph.2021.108075

Zhao, F. Z., Li, Y. Y., Yuan, D. K., Tan, K. W., and Sun, J. (2025). Wave influence on water circulation and self-purification ability in a semi-enclosed sea. *Continental Shelf Res.* 289, 1–13. doi: 10.1016/j.csr.2025.105461

Zheng, S., Edmonds, D. A., Wu, B., and Han, S. (2019). Backwater controls on the evolution and avulsion of the Qingshuigou channel on the Yellow River Delta. *Geomorphology* 333, 137–151. doi: 10.1016/j.geomorph.2019.02.032

Zheng, S., Wu, B., Wang, K., Tan, G., Han, S., and Thorne, C. R. (2017). Evolution of the Yellow River delta, China: Impacts of channel avulsion and progradation. *Int. J. Sediment Res.* 32, 34–44. doi: 10.1016/j.ijsrc.2016.10.001

Zhou, L. Y., Liu, J., Saito, Y., Diao, S. B., Gao, M. S., Qiu, J. D., et al. (2020). Sediment budget of the Yellow River delta during 1959-2012, estimated from morphological changes and accumulation rates. *Mar. Geology* 430, 1–14. doi: 10.1016/j.margeo.2020.106363

Zhu, L., Hu, R., Zhu, H., Jiang, S., Xu, Y., and Wang, N. (2018). Modeling studies of tidal dynamics and the associated responses to coastline changes in the Bohai Sea, China. *Ocean Dynamics* 68, 1625–1648. doi: 10.1007/s10236-018-1212-2